Chemical Science

Accepted Manuscript

This article can be cited before page numbers have been issued, to do this please use: B. feng, K. Shen, C. Chen, J. Zhang, F. Chen, Y. Li, J. Yu, C. Liu, X. Wang and H. Chen, *Chem. Sci.*, 2026, DOI: 10.1039/D6SC02768G.

ROYAL SOCIETY OF CHEMISTRY

rsc.li/chemical-science

View Article Online
DOI: 10.1039/D6SC02768G

ARTICLE

Received 00th January 20xx,
Accepted 00th January 20xx
DOI: 10.1039/x0xx00000x

EMM-17 as an efficient catalyst for the one-step conversion of high-concentration lactic acid into lactide

Binyao Feng, [†a] Kunhao Shen, [†a] Chenxu Liu, [ab] Xingrui Wang, [c] Cailing Chen, [b] Jian Zhang, [d] Huiyong Chen, [c] Feijian Chen, *[ab] Yi Li, *[ab] Jihong Yu *[ab]

As the key precursor for biodegradable polylactic acid (PLA), lactide (LT) is vital for sustainable polymer development, but its preparation in industry still relies on the traditional two-step process involving harsh conditions of high temperature and high vacuum with limited yield. The recently developed one-step approach based on heterogeneous catalysts (e.g., Beta zeolite) shows promising potential as a viable route, but its feasibility crucially depends on the development of highly efficient catalysts. In this work, the aluminosilicate zeolite EMM-17 featuring 11-ring channels was introduced as a novel catalyst for the conversion of 105 wt.% lactic acid (LA) for the first time, achieving record-breaking performance, with an LA conversion reaching 98% and an LT yield of 91%, substantially outperforming previously reported zeolite-based catalysts. By selective silylation of acid sites on the external surface of EMM-17, together with composition analysis of the product and density functional theory (DFT) calculations, it demonstrates that such superior catalytic performance of EMM-17 is derived from its unique external surface acid sites, which effectively promote the conversion of L_nA (n≥3) oligomers into LT and smaller substrates within high-concentration LA systems.

Introduction

With the growing severity of white pollution, the development and promotion of biodegradable materials to replace traditional petroleum-based plastics is urgently required to achieve global sustainable development goals.[1-8]Among numerous degradable materials, polylactic acid (PLA) is regarded as one of the most promising alternatives due to its excellent biodegradability, biocompatibility, and mechanical properties.[9-11] As the key intermediate in synthesizing high-quality PLA, the production costs and product purity of lactide (LT) directly determine the market competitiveness of PLA products.[12-15] The conventional two-step process is currently widely employed in industry for the preparation of LT. A lactic acid prepolymer is first prepared through the dehydrative polycondensation of aqueous lactic acid solution, and then undergoes intramolecular lactonization to generate LT.[16, 17] However, this process exhibits significant drawbacks: on the one hand, racemization during the reaction diminishes the selectivity of LT; on the other hand, the reaction necessitates harsh conditions of high temperature and high vacuum, resulting not only in high energy consumption but also limited yield.[14, 18, 19] To overcome these shortcomings, researchers have developed an entirely novel one-step conversion of lactic acid (LA) for synthesizing LT. Compared to the traditional two-step approach, this one-step process offers distinct advantages including simpler procedures, milder reaction conditions, significantly reduced energy consumption, and an effective improvement in LT yield. [20]

The core of the one-step method for producing LT from LA lies in the development of highly efficient catalysts. Conventional homogeneous catalysts face challenges of difficult recovery and poor recyclability, whereas zeolites, as a class of highly efficient, recyclable heterogeneous catalysts, [21 22 23] demonstrate significant potential for the one-step synthesis of LT directly from LA.[14, 24, 25] In 2015, Dusselier *et al*. first proposed an one-step continuous dehydration process for LA based on zeolite catalysts.[20] Studies have confirmed that this process presents several key advantages: a shorter synthetic route, a lower reaction temperature, and higher product purity, while Beta zeolites exhibit excellent selectivity for LT synthesis. Subsequently, Beta zeolites and their modified catalyst materials have become a research focus in this field in recent years. For instance, Beta nanocrystals with low Si/Al ratios synthesized by Yu et al. achieved a high conversion of 105 wt.% LA to LT, with a LT yield reaching 74%.[26] Hierarchical Beta zeolites, owing to their interconnected micro-mesoporous structure, effectively shorten the diffusion pathways for LT within the pore channels, thereby reducing side reactions and simultaneously enabling high-yield synthesis of LT.[27-29] Moreover, the catalytic performance was further enhanced by increasing the number of active sites through the incorporation of heteroatoms (Ti, Sn) into the zeolite.[30-32] In addition to Beta zeolites,

[a.] *State Key Laboratory of Inorganic Synthesis and Preparative Chemistry, College of Chemistry, Jilin University, Changchun 130012, P. R. China*
***E-mail:** jihong@jlu.edu.cn; yili@jlu.edu.cn; feijian@jlu.edu.cn*
[b.] *International Center of Future Science, Jilin University, Changchun 130012, P. R. China*
[c.] *School of Chemical Engineering, Northwest University, Xi'an, Shaanxi 710069, P. R. China*
[d.] *Beijing Advanced Innovation Center for Soft Matter, Science and Engineering, Beijing University of Chemical Technology, Beijing, P. R. China*
† These authors contributed equally to this work.
Supplementary Information available: [details of any supplementary information available should be included here]. See DOI: 10.1039/x0xx00000x

researchers have also explored other topological structures of zeolites. For example, the ITQ-47 (**BOG**) zeolites show a high LA conversion with a 73.7% LT yield in an o-xylene system.[33] Al-substituted IPC-4 zeolites also exhibited a higher LT selectivity comparable to that of commercial Beta zeolites in the para-xylene system, that is, above 55%.[34] However, current research efforts predominantly focus on the synthetic regulation or heteroatom doping modification of Beta zeolites. Although such strategies can enhance catalytic performance to some degree, they often involve complex synthetic procedures, which substantially raise the cost and difficulty of preparation, thereby restricting the large-scale application of the catalysts.[35, 36]

The recently developed aluminosilicate zeolites EMM-17 possess a three dimension (3D) 11 × 10 × 10 membered-ring (MR) pore openings similar to that of Beta zeolites, albeit slightly smaller.[37, 38] Notably, in this work we present that in the catalytic production of LT from 105 wt.% LA, the EMM-17 zeolite synthesized solely via conventional hydrothermal methods demonstrated superior performance compared to commercial Beta zeolites and all previously reported zeolite catalysts without further modification, achieving an LT yield as high as 91%. To elucidate the origin of outstanding catalytic performance of EMM-17, we employed tributylchlorosilane (TBCS) matching the pore channels of EMM-17 for silylation. This achieved selective removal of acid sites on the external surface of EMM-17 (where calcination replaced H^+ sites with Si to form Si−OH bonds), while preserving acid sites within the pores. DFT calculations were also employed to simulate the reaction energy barriers on the external surface and within the pore channels, yielding conclusion consistent with experimental results. It was found that the acid sites on EMM-17 external surface efficiently promote the conversion of L_nA (n≥3) to form LT and the monomer LA or LA dimer(L_2A). Subsequently, L_2A can enter the micropore channels within EMM-17 easily, whose dimensions not only optimize the process of LT formation but also effectively suppress the hydrolysis side reaction of LT. In summary, this work not only for the first time developed EMM-17 as a highly efficient novel catalyst for the conversion of LA to LT, but also profoundly unveiled the pivotal role of its structural characteristics and external surface acid sites in shape-selective catalytic reactions. This provides crucial evidence for the in-depth investigation and lays an important foundation for the further development and application of EMM-17.

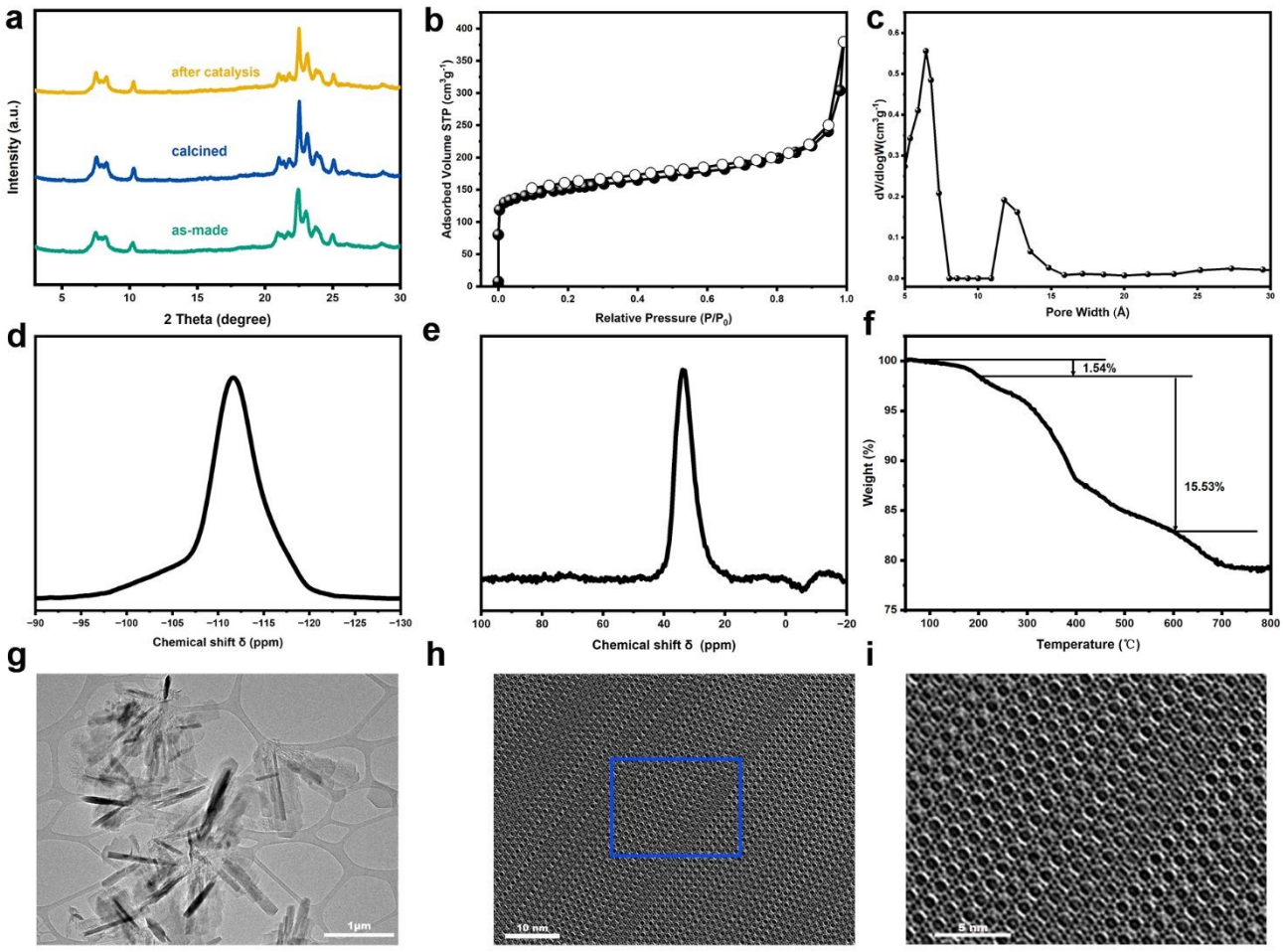

Fig.1 (a) PXRD patterns, (b) N_2 adsorption-desorption isotherms, (c) pore size distribution profile, (d) ^{29}Si MAS NMR and (e) ^{27}Al MAS NMR spectra, (f) TG curve, (g) TEM image and (h) iDPC-STEM image of EMM-17, and (i) enlarged image within the blue frame area.

View Article Online
DOI: 10.1039/D6SC02768G

ARTICLE

Results and discussion

EMM-17 zeolites were synthesized via the hydrothermal method with 1-ethyl-4-(pyrrolidin-1-yl) pyridine-1-ium hydroxide as the organic structure-directing agents (OSDA). The typical gels with a composition of SiO_2: 0.8 OSDAOH: 0.0167 Al_2O_3: 0.8 HF: 5 H_2O were selected and crystallized at 160°C for 5 days in a 3 mL Teflon-lined stainless steel autoclave. The target solid products were obtained following washing treatments with ethanol and deionized water as well as centrifugation. Afterward, the sample was dried overnight at 80 °C, and then calcinated at 550 °C for 8 hours to remove the OSDA thoroughly. Subsequently, a series of physicochemical characterizations were carried out on EMM-17. Powder X-ray diffraction (PXRD) analysis was conducted on EMM-17 zeolites before and after calcination, as well as following catalytic reactions (Fig. 1a). The results revealed distinct characteristic diffraction peaks for EMM-17 in all samples, indicating that the zeolite maintained excellent crystallinity and outstanding stability throughout the preparation and reaction processes. The N_2 adsorption-desorption isotherm (Fig. 1b) indicates that the adsorption capacity of EMM-17 increases rapidly at relative pressures $P/P_o < 0.1$, exhibiting typical characteristics of a microporous material, with a specific Brunauer-Emmett-Teller (BET) surface area of 566 m^2/g and a micropore volume of approximately 0.18 cm^3/g. The pore size distribution calculated by nonlocal density functional theory (NLDFT) (Fig. 1c) implies that, in addition to micropores, a small amount of mesopores present in EMM-17. The coordination environments of silicon and aluminium in EMM-17 were characterized by ^{29}Si Magic Angle Spinning Nuclear Magnetic Resonance (MAS NMR) and ^{27}Al MAS NMR. Fig. 1d reveals that silicon atoms in EMM-17 adopt a Q^4 coordination state, indicating a highly intact zeolite framework structure. The characteristic signal at 59 ppm of the ^{27}Al MAS NMR in Fig. 1e also confirms its tetracoordinated framework aluminium within the zeolite framework. And the thermogravimetric analysis (TG) curve for EMM-17 (Fig. 1f) shows a weight loss of 15.53 % within the 200–600 °C temperature range, attributable to the thermal decomposition of the OSDA within the zeolite. Scanning electron microscopy (SEM) images (Fig. S1) and transmission electron microscopy (TEM) images (Fig. 1g) reveal that EMM-17 comprises lamellar crystals approximately 1 μm in size. Integrated differential phase contrast scanning transmission electron microscopy (iDPC-STEM) images of EMM-17, acquired along the (010) direction (Fig. 1h-i), clearly demonstrate that it consists of polymorph A and polymorph B, coexisting in an approximate 1:1 ratio, exhibiting a well-defined 11-ring pore openings.

The prepared EMM-17 with a Si/Al ratio ≈ 30 was employed to catalyze the conversion of 105wt% LA to produce LT. Commercial Beta zeolites (denoted as Beta-C), industrially common ZSM-5 zeolites, Self-pillared pentasil zeolite (denoted as SPP) with a intergrowth structure, and mesoporous ZSM-5 (denoted as ZSM-5-M) were selected as comparative catalysts to evaluate the catalytic performance of EMM-17. A series of basic physical and chemical characterization were conducted on the comparative catalysts. The results showed that all the comparative catalysts had corresponding crystal structure characteristics (Fig. S2-S9, Table S1). Subsequently, NH_3-temperature programmed desorption (NH_3-TPD) and pyridine Fourier Transform Infrared Spectroscopy (Py-FTIR) tests were carried out to characterize their acidity (Fig. S10, S11). Then, the aforementioned catalysts were used to catalyze the one-step conversion of 105wt% LA to produce LT, in order to evaluate and compare their catalytic activities. The reaction pathway of LA to LT is as follows: LA first polymerizes to form a polymer (L_nA), wherein dimers (L_2A) may undergo further cyclisation to yield LT, or continue polymerizing to form higher molecular weight L_nA (n≥3) (Fig. S12).

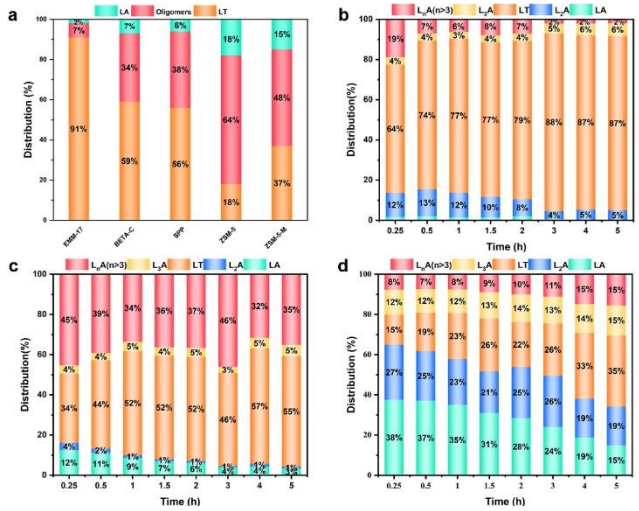

Fig.2 (a) Catalytic performance of various catalysts determined by ^1H NMR, and HPLC profiles of LA conversion over (b) EMM-17, (c) Beta-C and (d) EMM-17-S2. Reaction conditions: 1 g catalyst, 1 g LA (105wt%) and 12.5 ml toluene reaction for 5 h at 140 °C. Note: "Oligomers" in Fig.2 (a) refers to L_nA (n≥2)

The comparative results of the catalytic performance of different catalysts were shown in Fig. 2a and Fig. S13: Among the four comparison catalysts, the LT yield decreased in the order of Beta-C, SPP, ZSM-5-M, and ZSM-5, with Beta exhibiting superior catalytic performance. This finding is consistent with previously reported literature results. [20] The catalytic performance of EMM-17 surpassed all reference catalysts, achieving an LA conversion rate of 98% and a LT yield as high as 91%. In addition to the basic catalytic tests, the effects of the Si/Al ratio, solvent type and reaction temperature of EMM-17 on the catalytic performance were also investigated, and cyclic tests were conducted. (Figs.S14-S16). To gain deeper insights into the reaction process, high performance liquid chromatography (HPLC) was employed to monitor the evolution of each component

View Article Online DOI: 10.1039/D6SC02768C

with reaction time in the EMM-17 and commercial Beta zeolite catalytic systems (Fig. 2b and 2c). The results indicate that EMM-17 exhibited a faster initial reaction rate, with the LT yield reaching 63.9% after only 0.25 hours. With increasing reaction time, the LT yield rose steadily, and stabilized after 3 hours. It is noteworthy, however, that within the EMM-17 catalytic system, the content of polymers L_nA (n≥3) exhibited a decreasing trend with prolonged reaction time. In contrast, under the commercial Beta zeolite catalytic system, no significant tendency towards polymer conversion was observed. Given that the pore structure of EMM-17 prohibits the in-situ conversion of large polymer molecules, we hypothesize that distinct acid sites on its external surface can efficiently catalyze a surface pre-depolymerization process, thereby converting polymers into small-molecule products such as LA and L_2A. Subsequently, the small molecule products enter the pores of EMM-17 to participate in the generation reaction of LT.

To validate the role of acid sites on the external surface of EMM-17 in promoting polymer dissociation, selective passivation of these sites was carried out. To avoid pore blockage and mass transfer limitations caused by silica coating on the external surface, this study draws on the "single-atom passivation" strategy proposed by Liu's research group and employs the gas-phase silanization method, that is, one passivated atom selectively masks one protic acid site.[39] The TBCS with a larger kinetic diameter was selected as the silylation reagent to treat EMM-17. TBCS can selectively bind to the protonic acid sites (H^+) on the external surface of EMM-17 to form Si–C bonds and release HCl gas. After calcination treatment, the H^+ proton sites on the outer surface are replaced by Si atoms to form Si–OH, and the acidity disappears. Through optimization of the silylation treatment process, samples featuring selective passivation of external surface acid sites were successfully prepared (denoted as EMM-17-SX, where X is the number of silylation treatments). Characterization confirmed that samples subjected to silylation treatment retained the characteristic PXRD diffraction peaks of EMM-17, indicating that the silylation treatment did not disrupt the crystal structure of EMM-17 (Fig. S17a). The N_2 adsorption-desorption isotherm indicates that EMM-17-SX retains typical microporous characteristics. Compared to untreated EMM-17, EMM-17-SX exhibits a slight decrease in BET specific surface area, yet its microporous specific surface area and microporous volume remain largely unchanged (Fig. S17b, Table S2). SEM and TEM images showed that the samples after silylation treatment still maintained regular crystal morphology (Fig. S18, S19). To investigate the effect of silylation treatment on the acidic properties of EMM-17, a series of acid characterization studies were conducted on both EMM-17 and EMM-17-SX. The results of NH_3-TPD show that the desorption peaks at 150-250°C and 350-450°C corresponded to the weak acid and strong acid sites of the samples, respectively. After silylation treatment, the signal peak of EMM-17-SX shifted towards the low-temperature zone and the peak area decreased, indicating that the acid intensity of EMM-17-SX weakened and the acid amount decreased (Fig. 3a, Fig. S20). Catalytic performance tests were conducted on EMM-17, EMM-17-S1, and EMM-17-S2. The corresponding catalytic performance was illustrated in the Fig. S21, Fig. S22, and Fig. 2b, 2d. As the number of silylation treatments increased, the yield of LT exhibited a decreasing trend, and a gradual increase in the proportion of polymeric products within the system could be clearly observed. It is worth noting that EMM-17-S1 still retains a certain ability for polymers conversion, whereas EMM-17-S2 has largely lost this ability and even exhibits difficulty in converting LA. Subsequently, a series of characterization studies were conducted on EMM-17-S2. ^{29}Si MAS NMR and ^{27}Al MAS NMR analyses of EMM-17-S2 revealed that the coordination environments of Si and Al remained unchanged after two rounds of silylation treatment (Fig. S23). The Py-FTIR spectrum at 150°C desorption temperature (Fig. 3b, Fig. S24) indicates no significant change in the Brønsted acid (B acid, 1545 cm^{-1}) and Lewis acid (L acid, 1455 cm^{-1}) content between the pre- and post-treatment samples.

To further determine the successful coverage of acid sites on the external surface of EMM-17 by silylation treatment, characterization was carried out by 2,4, 6-tert-butylpyridine FTIR. Since the molecular size of TTBP is larger than the micropore size of EMM-17 zeolite, it can only interact with the acid sites on the external surface of EMM-17. The signal of chemically adsorbed TTBP was detected by *in-situ* FT-IR spectroscopy.[40, 41] As shown in Fig. 3c and 3d, the characteristic absorption signals of EMM-17 were observed at 1611 cm^{-1} and 3644 cm^{-1}, which were related to the ring vibration of the protonated $TTBPH^+$ and the N–H stretching vibration peak. No obvious absorption signals were detected for EMM-17-S2 at the aforementioned wavenumbers, suggesting the near-complete absence of acid sites on its external surface. This result verifies that the silylation treatment has effectively passivated the external acid sites of EMM-17. Catalytic performance evaluation (Fig. 2d) revealed that the LT yield over EMM-17-S2 dropped markedly, accompanied by significant accumulation of polymeric species (L_nA, n≥3) in the reaction system. This observation further validates that the external acid sites of EMM-17 serve a critical function in the pre-depolymerization of polymers in concentrated LA systems, and thus represent a key contributor to its superior catalytic activity.

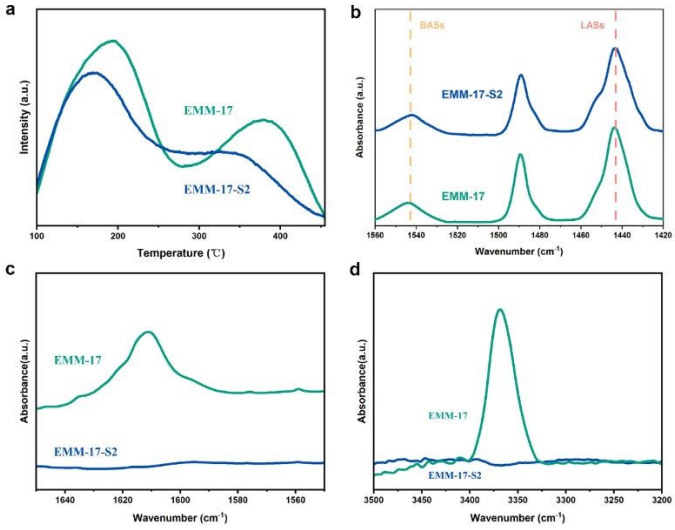

Fig.3 (a) NH_3-TPD curves, (b) Py-FTIR spectra of EMM-17 and EMM-17-S2, TTBP-FTIR spectra in the range of (c) 1650–1550 and (d) 3500–3200 cm^{-1} of EMM-17 and EMM-17-S2.

View Article Online
DOI: 10.1039/D6SC03768C

Based on the TEM results, the [010] crystal plane of the EMM-17 was chosen. According to its structural geometry, 6 potential reactive T-sites were identified in EMM-17A (pure polymorph A) and EMM-17B (pure polymorph B), and their adsorption energies were calculated accordingly. A lower adsorption energy corresponds to stronger adsorption affinity. As summarized in Tables S3 and S4, the T5 site in EMM-17A and the T15 site in EMM-17B displayed distinct superiority in adsorption energy. As depicted in Fig. S25, both sites are situated at the intersection of the straight channels.

The Gibbs free energies of the conversion of L_3A and L_4A over the external surface of EMM-17 were calculated and compared. Firstly, the energy barriers of different conversion pathways of L_3A and L_4A on the external surface of EMM-17A were calculated, as shown in Fig. 4a and 4b. On this surface, L_3A and L_4A preferentially undergo direct conversion to LT and LA (or L_2A), with energy barriers of 36.79 and 31.98 kJ/mol, respectively. These values are markedly lower than the energy barriers of 79.69 and 117.64 kJ/mol required for the hydrolytic transformation of L_3A and L_4A into L_2A. Similarly, direct formation of LT from L_3A and L_4A remains the dominant pathway over EMM-17B. Notably, however, L_3A conversion on EMM-17B proceeds with significantly higher efficiency, whereas the energy barrier for L_4A conversion reaches 94.52 kJ/mol, which is much higher than that of EMM-17A. Results show that regardless of whether L_3A and L_4A are converted to LT and LA, or exclusively to L_2A, the reaction rates of all four pathways are positive, indicating they are thermodynamically feasible. Although the hydrolysis energy barriers on the external surface are relatively high, they still have the possibility to occur. The possible reasons are shown as follows: when L_nA (n≥3) forms a hydrogen bond network with the Brønsted acid site in a locally bent form, it is conducive to the conversion to LT; When the ester oxygen of L_nA (n≥3) is co-adsorbed with water at the Brønsted acid site, hydrolysis may occur.

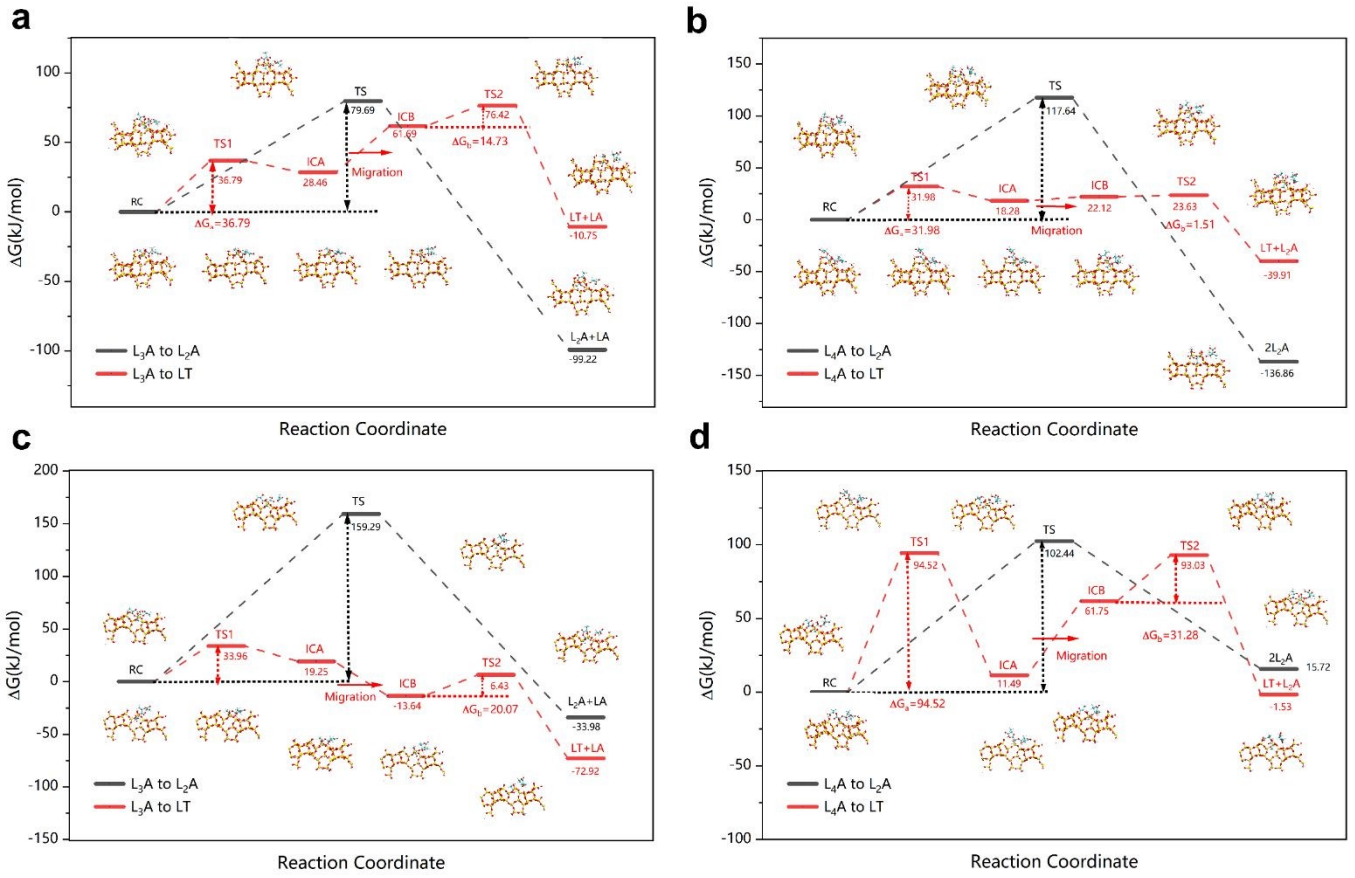

Fig.4 Free energy profiles of the conversion of L_3A and L_4A to LT or L_2A on the external surface of (a, b) EMM-17A and (c, d) EMM-17B.

Fig. S26a gives the PBE/PAW optimized structures of species participating in the formation of LT through L_3A and L_4A over EMM-17A, respectively. In the initial reactant complex (**RC**), a stable hydrogen bond (H-bond) network is formed between the L_3A substrate and EMM-17. Specifically, the carbonyl oxygen of the C_2=O group in L_3A forms an H-bond with an acidic proton, with an O···H distance of 1.942 Å; concurrently, the O1-H group in L_3A forms an H-bond with the zeolite oxygen (O_4). Starting from **RC**, the nucleophilic attack of O_1 (from L_3A) on the carbonyl carbon C_2 is coupled with a double proton transfer process, corresponding to the transition state **TS1**. In this step, the negatively charged O_4 acts as a basic site to abstract the proton from the O_1-H group, while the acidic proton from O_5-H serves as an acidic site to donate a proton to the carbonyl oxygen O_2. This highly synergistic acid-base catalysis drives the formation of the intermediate **ICa**, in which the C_2-O_1 bond is already formed. To facilitate the subsequent cleavage of the C_2-O_3 bond, the

View Article Online
DOI: 10.1039/D5SC02756C

H-bond network in **ICa** must reorient to the configuration observed in **ICb**. In **ICb**, the acidic proton from O_4-H maintains an H-bond with O_3, with an O_3···H distance of 1.578 Å. Similarly, the general acid-base catalysis mediated by EMM-17 via transition state **TS2** triggers the cleavage of the C_2-O_3 bond, ultimately yielding the final products LT and LA (product complex, **PC**). The reaction pathway for the conversion of L_4A to LT over EMM-17A and the conversion of L_3A and L_4A to LT over EMM-17B are analogous to that described above (Fig. S26b and Fig. S28). Additionally, an optimized structure for the hydrolysis reaction—where L_3A and L_4A are converted exclusively to L_2A without LT generation—was constructed (see Fig. S27 and Fig. S29).

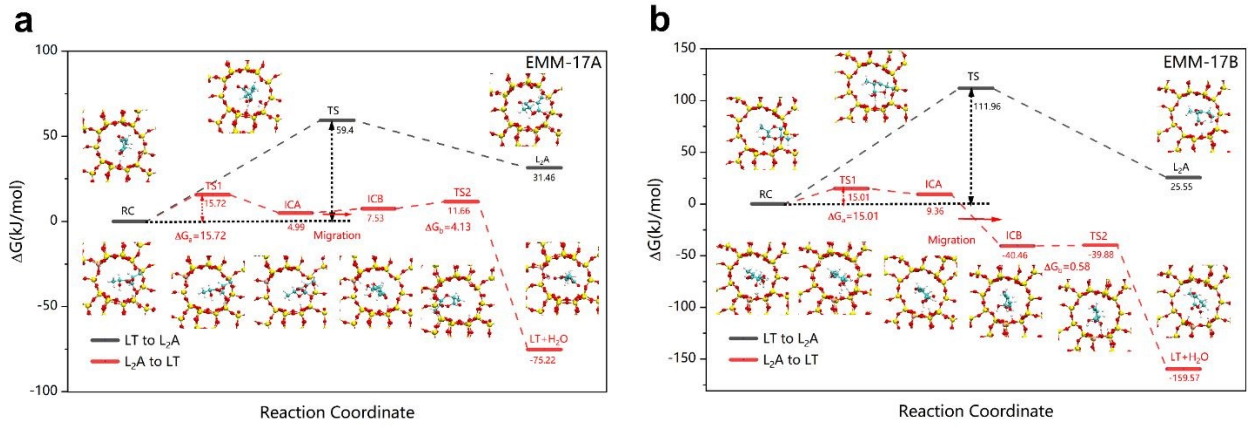

Fig.5 Free energy profiles of the conversion of LT to L_2A and L_2A to LT in the pore of (a) EMM-17A and (b) EMM-17B.

In addition, the energy barriers for the reactions when L_2A enters the EMM-17 pore channel were also calculated. As shown in Fig. 5, the energy barriers for the formation of LT in the EMM-17 pore channel by L_2A were 15.72 kJ/mol and 15.01 kJ/mol, respectively. For the side reaction of the hydrolysis of the generated LT to form L_2A, the corresponding energy barriers were as high as 59.4 kJ/mol and 111.96 kJ/mol. It can be understood that the unique 11-ring pore channel structure of EMM-17 can effectively restrict the formation of LT to L_2A, thereby further increasing the yield of LT.

Furthermore, we also calculated the energy barriers for the catalytic conversion of L_3A and L_4A by the external surface of Beta zeolite and compared them with EMM-17. As shown in Fig. S30 and Table S5, Beta only exhibited a slight advantage in the reaction pathway of catalysing the hydrolysis of L_4A to generate L_2A. In all other reaction pathways, EMM-17 showed an advantage, which explains the reason why the catalytic performance of EMM-17 is superior to that of Beta.

In conclusion, based on the existing experimental data, it is proved that the external surface of EMM-17 can effectively catalyze the conversion of L_3A and L_4A into LT. With the participation of water, it can also be hydrolysed into L_2A and diffuse into the pores for reaction, and it also shows excellent catalytic performance in the pores.

Conclusions

In this work, we selected the EMM-17, an aluminosilicate zeolite with an 11-ring channel structure, as the catalyst for the one-step conversion of LT from high-concentration LA. EMM-17 demonstrated excellent catalytic performance with a 98% LA conversion and a 91% LT yield, surpassing all previously reported zeolite catalysts. Subsequently, we combined the silylation treatment experiments and theoretical calculations to investigate the acid sites on external surface and pore structure characteristics of EMM-17: The unique 11-ring pore effectively enhanced the selectivity of EMM-17 in catalysis, while the exposed acidic sites on its external surface endowed EMM-17 with the ability to efficiently catalyse high-concentration LA reaction systems containing a large amount of L_nA (n≥3). This work not only provides a new catalyst for the preparation of LT from LA, but also explores the reasons for its high activity, and provides a theoretical basis for subsequent catalytic applications of EMM-17, especially in the exploration of the field of macromolecular catalysis.

Author contributions

†These authors contributed equally. B. Feng designed and conducted the experiments, performed the data analysis, and drafted the manuscript; K. Shen conducted theoretical calculations; C. Liu characterized samples, and provided some suggestions to improve the work; X. Wang performed silylation of samples; C. Chen performed iDPC-STEM imaging analysis; J. Zhang performed TTBP-FTIR tests; H. Chen conducted silylation of samples and data analysis; Y. Li supervised the theoretical calculations; F. Chen was responsible for the supervision, manuscript revision, and funding acquisition; J. Yu conceived and supervised the research, and contributed to manuscript revision, and funding acquisition.

Conflicts of interest

There are no conflicts to declare.

Data availability

The data supporting this article have been included as part of the Supplementary Information.

Acknowledgements

We thank the National Key Research and Development Program of China (Grant 2022YFA1503600), the National Natural Science Foundation of China (Grants 22288101, 22425201, and 22271115), the Fundamental and Interdisciplinary Disciplines Breakthrough Plan of the Ministry of Education of China (JYB2025XDXM903), the '111 Center' (B17020), and the Natural Science Foundation of Jilin Province (20230101355JC).

References

1. M. MacLeod, H. P. H. Arp, M. B. Tekman and A. Jahnke, *Science*, 2021, **373**, 61-65.
2. R. A. Sheldon and M. Norton, *Green Chem.*, 2020, **22**, 6310-6322.
3. V. Nagarajan, A. K. Mohanty and M. Misra, *ACS Sustainable Chem. Eng.*, 2016, **4**, 2899-2916.
4. W.-J. Yi, L.-J. Li, Z. Hao, M. Jiang, C. Lu, Y. Shen and Z.-S. Chao, *Ind. Eng. Chem. Res.*, 2017, **56**, 4867-4877.
5. X. Tang and E. Y. X. Chen, *Chem*, 2019, **5**, 284-312.
6. G. W. Coates and Y. D. Y. L. Getzler, *Nat. Rev. Mater.*, 2020, **5**, 501-516.
7. J. M. Garcia and M. L. Robertson, *Science*, 2017, **358**, 870-872.
8. T. P. Haider, C. Völker, J. Kramm, K. Landfester and F. R. Wurm, *Angew. Chem., Int. Ed.*, 2019, **58**, 50-62.
9. J. Muller, C. González-Martínez and A. Chiralt, *Materials*, 2017, **10**, 952.
10. S. Farah, D. G. Anderson and R. Langer, *Adv. Drug Delivery Rev.*, 2016, **107**, 367-392.
11. W. Ali, H. Ali, S. Gillani, P. Zinck and S. Souissi, *Environ. Chem. Lett.*, 2023, **21**, 1761-1786.
12. M. Singhvi and D. Gokhale, *RSC Adv.*, 2013, **3**, 13558-13568.
13. C. Gonçalves, I. C. Gonçalves, F. D. Magalhães and A. M. Pinto, *Polymers*, 2017, **9**, 269.
14. L. Shen, E. Worrell and M. Patel, *Biofuels, Bioprod. Biorefin.*, 2010, **4**, 25-40.
15. X. Meng, Y. Zhang, H. Zhou and L. Yu, *ACS Sustainable Chem. Eng*, 2022, **10**, 7658-7663.
16. X. Meng, L. Yu, Y. Cao, X. Zhang and Y. Zhang, *Org. Biomol. Chem.*, 2021, **19**, 10288-10295.
17. O. Dechy-Cabaret, B. Martin-Vaca and D. Bourissou, *Chem. Rev.*, 2004, **104**, 6147-6176.
18. M. Dusselier, P. Van Wouwe, A. Dewaele, E. Makshina and B. F. Sels, *Energy Environ. Sci.*, 2013, **6**, 1415-1442.
19. P. Van Wouwe, M. Dusselier, E. Vanleeuw and B. Sels, *ChemSusChem*, 2016, **9**, 907-921.
20. M. Dusselier, P. Van Wouwe, A. Dewaele, P. A. Jacobs and B. F. Sels, *Science*, 2015, **349**, 78-80.
21. Q. Zhang, J. Li, G. He, J. Li, Z. Chen, Q. Zhang, C. Wang, G. Qi, Q. Wang, P. Zhang, J. Xu, O. Terasaki, D. Mei, Z. Liu and J. Yu, *CCS Chem.*, 2025, **7**, 819-831.
22. M. Gao, G. Yang, G. He, R. Bai, J. Li, Y. Liu, Q. Zhang, G. Chen, D. Mei and J. Yu, *CCS Chem.*, 2024, **6**, 652-662.
23. J. Han, J. Li, Y. Bai, Y. Wei, D. Li, W. Yan and J. Yu, *CCS Chem.*, 2025, **7**, 681-690.
24. W. Groot, J. van Krieken, O. Sliekersl and S. de Vos, in *Poly(Lactic Acid)*, 2010, https://doi.org/https://doi.org/10.1002/9780470649848.ch1, pp. 1-18.
25. P. P. Upare, J. W. Yoon, D. W. Hwang, U. H. Lee, Y. K. Hwang, D.-Y. Hong, J. C. Kim, J. H. Lee, S. K. Kwak, H. Shin, H. Kim and J.-S. Chang, *Green Chem.*, 2016, **18**, 5978-5983.
26. Q. Zhang, S. Xiang, Q. Zhang, B. Wang, A. Mayoral, W. Liu, Y. Wang, Y. Liu, J. Shi, G. Yang, J. Luo, X. Chen, O. Terasaki, J.-P. Gilson and J. Yu, *Chem. Mater.*, 2020, **32**, 751-758.
27. X.-J. Chen, X. Hong, B. Zhan and X.-F. Hou, *Microporous Mesoporous Mater.*, 2024, **378**, 113250.
28. Y. Wang, J. Li, W. Tong, Z. Shen, L. Li, Q. Zhang and J. Yu, *Inorg. Chem. Front.*, 2022, **9**, 2470-2478.
29. Z. Ma, Q. Zhang, L. Li, M. Chen, J. Li and J. Yu, *Chem. Sci.*, 2022, **13**, 8052-8059.
30. R. De Clercq, M. Dusselier, C. Poleunis, D. P. Debecker, L. Giebeler, S. Oswald, E. Makshina and B. F. Sels, *ACS Catal.*, 2018, **8**, 8130-8139.
31. Y. Xu, Y. Fang, J. Cao, P. Sun, C. Min, Y. Qi, W. Jiang and Q. Zhang, *Ind. Eng. Chem. Res.*, 2021, **60**, 13534-13541.
32. L. Gao, K. Du, T. Yan, H. Li, D. Pan, Y. Zhang and Y. Tang, *Chem. Commun.*, 2022, **58**, 4627-4630.
33. Q. Huang, N. Chen, L. Liu, K. S. Arias, S. Iborra, X. Yi, C. Ma, W. Liang, A. Zheng, C. Zhang, J. Hu, Z. Cai, Y. Liu, J. Jiang and A. Corma, *Chem. Sci.*, 2020, **11**, 12103-12108.
34. I. Podolean, B. Cojocaru, V. I. Pârvulescu, M. Mazur, S. Abdi and J. Čejka, *Appl. Catal., A*, 2023, **665**, 119379.
35. Q. Huang, R. Li, G. Fu and J. Jiang, Crystals, 2020, 10, 781.
36. X. Ma, H. Guo, Y. Sui, Y. Li and J. Cao, *Asia-Pac. J. Chem. Eng.*, 2025, **20**, e70045.
37. S. C. Weston, B. K. Peterson, J. E. Gatt, W. W. Lonergan, H. B. Vroman, M. Afeworki, G. J. Kennedy, D. L. Dorset, M. D. Shannon and K. G. Strohmaier, *J. Am. Chem. Soc.*, 2019, **141**, 15910-15920.
38. X. Liu, L. Liu, T. Pan, N. Yan, X. Dong, Y. Li, L. Chen, P. Tian, Y. Han, P. Guo and Z. Liu, *Angew. Chem., Int. Ed.*, 2021, **60**, 24227-24233.
39. R. Liu, S. Zeng, T. Sun, S. Xu, Z. Yu, Y. Wei and Z. Liu, *ACS Catal.*, 2022, **12**, 4491-4500.
40. T. W. Beutel, A. M. Willard, C. Lee, M. S. Martinez and R. Dugan, *J. Phys. Chem. C*, 2021, **125**, 8518-8532.
41. H. K. Heinichen and W. F. Hölderich, *J. Catal.*, 1999, **185**, 408-414.

View Article Online
DOI: 10.1039/D6SC02768G

Data Availability Statement

All data associated with this article have been included in the main text and ESI†.